Korean J. Chem. Eng., 35(10), 1988-1993 (2018)
DOI: 10.1007/s11814-018-0109-6

pISSN: 0256-1115
eISSN: 1975-7220

Reduced graphene oxide supported V_2O_5-WO_3-TiO_2 catalysts for selective catalytic reduction of NOx

Minwoo Lee*,, Bora Ye*, Bora Jeong*, Hye-yeon Chun*, Duck Hyun Lee*, Sam-sik Park***, Heesoo Lee**, and Hong-Dae Kim*,†**

*Green Materials & Processes Group, Ulsan Regional Division, Korea Institute of Industrial Technology, Ulsan 44413, Korea
**Department of Materials Science and Engineering, Pusan National University, Busan 46142, Korea
***R&D Center, NANO. Co., Ltd., Sangju 37257, Korea
(*Received 12 March 2018 • accepted 24 June 2018*)

Abstract−We present a reduced-graphene-oxide (rGO)-supported V_2O_5-WO_3-TiO_2 (VWTi) catalysts for the efficient selective catalytic reduction of NOx. The rGO support provides well-dispersed functional sites for the nucleation of nanoparticles, allowing the formation of VWTi catalysts with high specific surface areas. The dispersion of the nanoparticles, as observed by transmission electron microscopy (TEM) and energy dispersive spectroscopy (EDS), confirmed the uniform dispersion of the particles on the rGO surface. Detailed Fourier-transform infrared (FT-IR) and NH_3 temperature-programmed desorption (NH_3-TPD) analyses indicated that the high density of acidic sites provided by the rGO is key to the observed enhancement of NOx removal efficiency, and the rGO-supported catalysts exhibit improved NOx removal efficiencies with smaller amounts of V_2O_5 and WO_3 compared with the commercially available V_2O_5-WO_3-TiO_2 catalysts.

Keywords: Reduced Graphene Oxide, NOx Removal Efficiency, Selective Catalytic Reduction, High Dispersion, Wet Impregnation

INTRODUCTION

Nitrogen oxide (NOx) produced during the combustion of fossil fuels at high temperature is considered to be a major cause of acid rain, smog, particulate matter, and global warming [1]. There have been numerous studies on the control of NOx emissions, and regulations regarding them are becoming more strict (IMO tier3, EURO6) [2,3]. Selective catalytic reduction (SCR) of NOx with ammonia (NH_3) is one of the most effective technologies for removing NOx from exhaust emissions [4]. Numerous metal-oxide-based SCR catalysts, such as V_2O_5-WO_3/TiO_2 [5-7], Fe/TiO_2 [8], CeO_2/TiO_2 [9] and MnOx/TiO_2 [10], have been studied in order to provide enhanced NOx removal, and the V_2O_5-WO_3/TiO_2 catalyst is widely used commercially because of its high catalytic activity, good thermal stability, and resistance to sulfur poisoning [11].

Vanadium oxide (V_2O_5) is the main catalytic component of the V_2O_5-WO_3/TiO_2 catalyst, and its content is generally limited to less than 2 wt% because higher content of V increases the production rate of N_2O, which is another form of NOx [12,13]. For high-sulfur applications, the content of V should be further reduced to less than 1 wt% to suppress the conversion of SO_2 to SO_3 [14]. Furthermore, V_2O_5 is known as a possible carcinogen, and occupational exposure limits are established in various countries, including Austria and the United States [15]. Likewise, high concentrations of WO_3 can have significantly negative effects on cell viability because of its neurotoxicity and dermal toxicity [16]. Thus, reducing the content of V_2O_5 and WO_3 in SCR catalysts while maintaining their NOx removal efficiency is a significant research challenge.

Graphene is a one-atom-thick two-dimensional layer of sp^2 hybridized carbon that possesses excellent mechanical and electrical properties as well as a high specific surface area [17-19]. It has been studied for many applications, including as electrochemical capacitors [20] and semiconductors [21]. Reduced graphene oxide (rGO) contains oxygen functional groups such as epoxides, alcohols, and carboxylic acids that can serve as well-dispersed, facile chemical functionalization sites [22]. Herein, we prepared V_2O_5-WO_3-TiO_2 (VWTi) catalysts containing reduced amounts of metal oxides and with higher NOx removal efficiencies by adopting rGO as a catalyst support. The rGO support provides functional sites for the nucleation of nanoparticles, and the catalytic activity of the catalyst was enhanced because of the high dispersion and the increased specific surface area. The NOx removal efficiency of the well-dispersed catalyst is enhanced because the dispersion of the densified components and the acid sites is closely related to the catalytic reaction [23].

EXPERIMENTAL DETAILS

1. Preparation of V_2O_5-WO_3-TiO_2 Catalysts

The reference catalyst 1V6W/Ti was prepared with 1 wt% V and 6 wt% W (see Table 1), which represents a similar elemental ratio to that of commercially available catalysts. The sample names indicate the compositions of the catalysts. For example, the label 1V6W indicates that the catalyst was prepared with 1 wt% V and 6 wt% W.

†To whom correspondence should be addressed.
E-mail: hdkim@kitech.re.kr

Table 1. Elemental compositions (in wt%) of the prepared catalysts

Samples	Ti	V	W	O	C
1V6W/Ti	60.8	0.8	5.6	32.8	-
1V6WTi/rGO	48.3	0.9	5.2	31.6	14.0
0.5V6WTi/rGO	57.2	0.5	4.3	26.5	11.5
1V3WTi/rGO	53.3	0.9	2.6	30.5	12.7
0.5V3WTi/rGO	49.4	0.5	2.7	37.0	10.4

rGO-supported V_2O_5-WO_3-TiO_2 catalysts were prepared by the wet impregnation method. The raw material of rGO (STANDARD GRAPHENE Inc., S. Korea) was purchased and used without any further treatment. A V solution was prepared by dissolving 0.5-1 wt% ammonium metavanadate (NH_4VO_3, Sigma-Aldrich, 99.99%) and oxalic acid (molar ratio 1 : 3) in deionized water (DI water) [24]. A W solution was prepared by dissolving 3-6 wt% ammonium metatungstate ($(NH_4)_6H_2W_{12}O_{40}\cdot xH_2O$, Sigma-Aldrich, 99.99%) in DI water. The same amount of TiO_2 (Sigma-Aldrich, 99.5%) was added to the prepared catalysts, and the solutions were mixed with a magnetic stirrer for 1 h at 40 °C. The prepared mixtures were added to an rGO dispersion (10 wt%) and stirred for 7 h at 60 °C for the impregnation process. The mixtures were dried on a rotary vacuum evaporator at 40 °C [25]. After drying, the catalyst powders were heat treated at 500 °C under a N_2 atmosphere for 2 h.

2. Catalytic Activity Measurements

The catalytic activity of the prepared catalysts was investigated using a fixed-bed reactor with continuous gas flow. A sample of a prepared catalyst (0.3 g) was loaded into the reactor, and a gas mixture composed of 300 ppm NO, 360 ppm NH_3, 5 vol% O_2, and N_2 balance was flowed at a total flow rate of 300 sccm and a space velocity of 60,000 mL g·cat^{-1} h^{-1}. Note that the NH_3/NOx molar ratio (α) was fixed at 1.2 to determine the highest efficiency of the catalysts with minimized ammonia slip [26]. The NOx concentration of the inlet and outlet was measured with a chemiluminescence detector (CLD, Teledyne T200H) analyzer at an operating temperature (T_{OP}) of $250 \le T_{OP} \le 500$ °C, and the NOx removal efficiency of the prepared catalysts was calculated using the following equation:

$$\text{NOx removal efficiency} = 100 \times \frac{\Delta\text{NOx}}{\text{NOx}_{inlet}}\% \quad (1)$$

where ΔNOx is the difference in NOx concentrations at the inlet and outlet of the reactor.

3. Characterization

The morphologies and elemental maps of the catalyst were obtained with transmission electron microscopy (TEM, JEOL, 2100F), scanning electron microscopy (SEM, Hitachi, SU8020), and their chemical compositions were analyzed with energy dispersive spectroscopy (EDS). X-ray diffraction (XRD, Rigaku, Ultima 4) measurements were performed using Cu Kα radiation (40 kV, 30 mA) at $20^\circ \le 2\theta \le 80^\circ$ in the continuous scan mode. Specific surface areas were measured using liquid N_2 adsorption at 77 K with a surface area analyzer (Micromeritics, ASAP 2020) and calculated using the Brunauer-Emmett-Teller (BET) method. The pore sizes and volumes were calculated using the Barrett-Joyner-Halenda (BJH) method. The surface-active-site densities were obtained using Fourier-transform infrared spectrometry (FT-IR, Varian, 670) and NH_3-temperature programmed desorption (NH_3-TPD, Micromeritics, Autochem II 2920). Raman spectroscopy measurements were also taken using Raman system (WITec, alpha300s) with excitation energy of 532 nm.

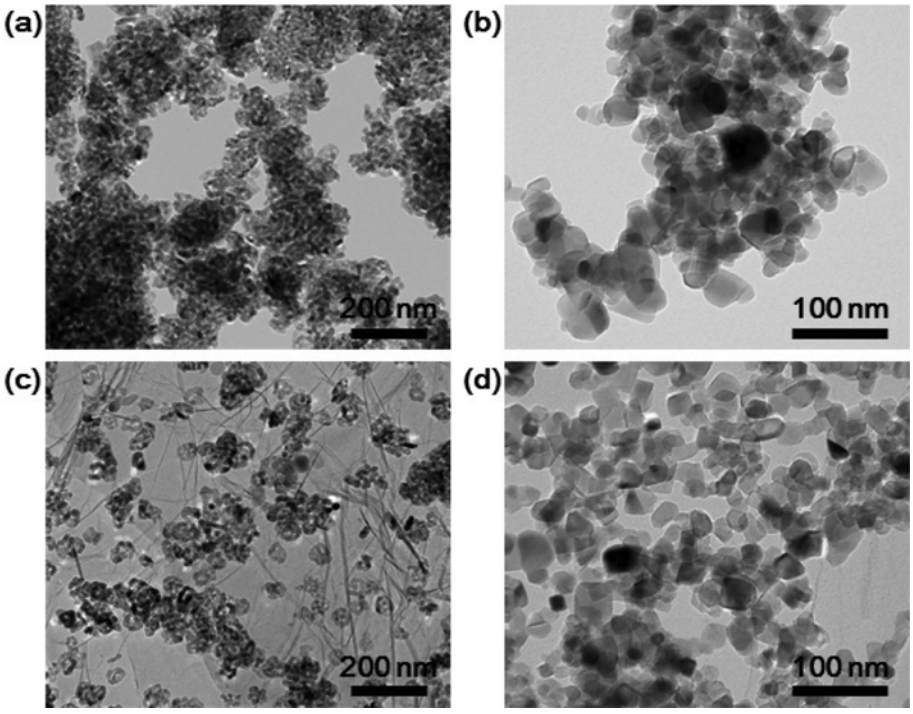

Fig. 1. Low- ((a) and (c)) and high-magnification ((b) and (d)) TEM images of the prepared 1V6W/Ti ((a) and (b)) and 1V6WTi/rGO ((c) and (d)) catalysts.

RESULTS AND DISCUSSION

1. Dispersion of Nanoparticles on rGO

Table 1 shows the elemental composition of the prepared catalysts as obtained from EDS measurements. Furthermore, the content of V and W in the prepared catalysts was confirmed to be similar to the intended content. Fig. 1 shows the low- and high-magnification TEM images of the prepared 1V6W/Ti (Figs. 1(a) and 1(b)) and 1V6WTi/rGO (Figs. 1(c) and 1(d)) catalysts. The TEM images of 1V6W/Ti show that the prepared metal oxide nanoparticles have diameters in the range 8-70 nm and that they are severely aggregated, forming large clusters of VWTi nanoparticles. The TEM images of the 1V6WTi/rGO catalyst show that the prepared VWTi nanoparticles are relatively well dispersed on the supporting rGO and have diameters in the range 20-50 nm. Although some particles are not supported on the rGO and are observed to have aggregated, this aggregation is significantly less common than that for the 1V6W/Ti catalyst. The dispersion of nanoparticles is due to the oxygen functional groups present on the rGO surface. The rGO was prepared by the reduction of GO using hydrazine hydrate vapor. However, this process does not completely reform the GO into pure graphene and leaves some oxygen groups remaining, even after prolonged exposure to hydrazine (Fig. S1). Thus, rGO provides enough functional sites for the nucleation of nanoparticles and leads to the formation of relatively well-dispersed and uniform VWTi nanoparticles. Fig. 2 shows the EDS mapping images of 1V6WTi/rGO for the elements C, O, Ti, V, and W, confirming that the prepared particles on the rGO are composed of vanadium oxide, tungsten oxide, and titanium oxide.

2. XRD Analysis and Surface Areas of the Prepared Catalysts

Fig. 3 shows the XRD patterns for the prepared catalysts with and without the rGO support. The measured patterns are attributed to anatase TiO_2 (JCPDS PDF 21-1272) crystal planes, showing reflections for 2θ values of 25.1° (101), 36.9° (103), 47.9° (200), 54.9° (211), 62.6° (204), 68.6° (116), 70.2° (220), and 74.9° (215) [27]. The rutile phase of TiO_2 (JCPDS, PDF 21-1276) is also observed from reflections with 2θ values of 27.2° (110), 36.0° (101), and 41.1° (111) [28]. It is well known that the activity of catalysts is dependent on the phase of TiO_2, and the anatase phase is the optimum structure for SCR because of its high specific area [29]. The XRD measurements clearly show that the TiO_2 particles maintain their anatase structure within the prepared catalysts. However, neither V_2O_5 nor WO_3 can be clearly observed owing to the very low V_2O_5 and WO_3 content of the catalysts. These species form small nanocrystals or amorphous particles on the surface of the rGO [30,31]. Consequently, we also obtained the compositions of the catalysts with X-ray fluorescence spectroscopy (XRF), confirming the formation of V_2O_5 and WO_3 (Table S2).

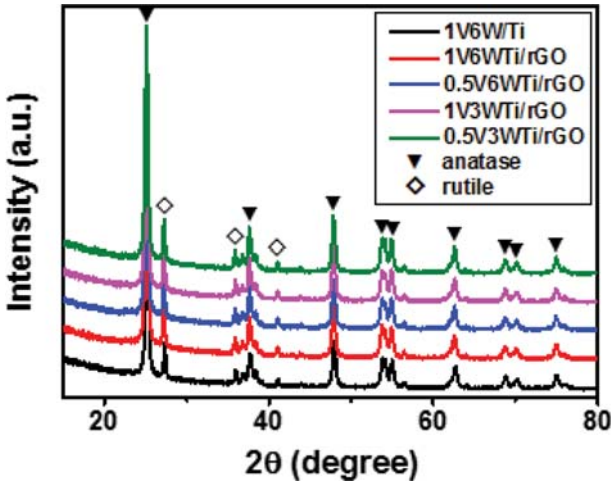

Fig. 3. X-ray diffraction patterns of the 1V6W/Ti (black), 1V6WTi/rGO (red), 0.5V6WTi/rGO (blue), 1V3WTi/rGO (magenta), and 0.5V3WTi/rGO (olive) catalysts.

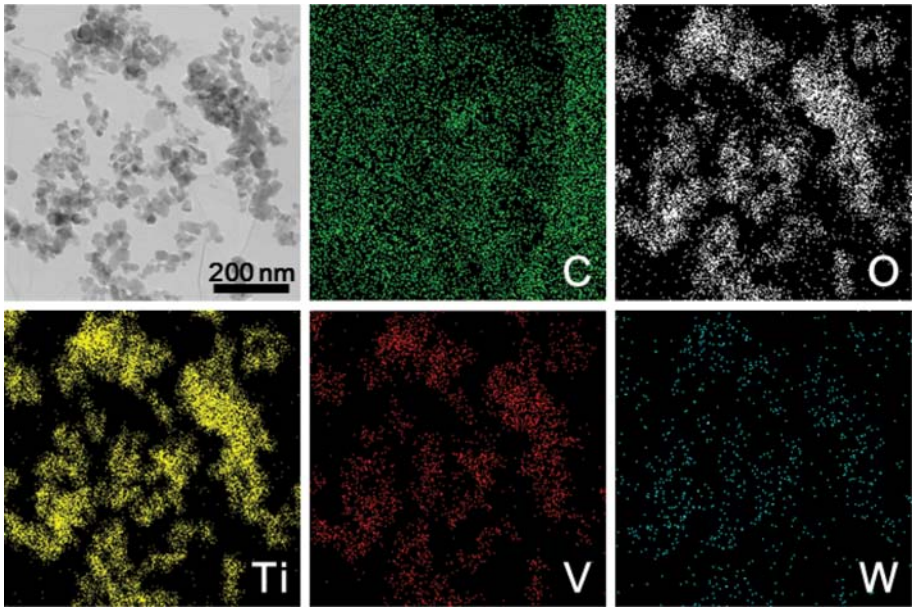

Fig. 2. TEM and element mapping images of the prepared 1V6WTi/rGO catalyst.

Table 2. Physicochemical properties of the prepared catalysts

Samples	S_{BET} [m^2g^{-1}]	Pore volume [cm^3g^{-1}]	Average pore size [nm]
1V6W/Ti	50.10	0.30	22.30
1V6WTi/rGO	74.20	0.33	16.30
0.5V6WTi/rGO	75.90	0.34	15.90
1V3WTi/rGO	77.30	0.29	13.70
0.5V3WTi/rGO	78.90	0.31	13.90

Table 2 shows the measured surface areas, pore volumes, and pore sizes of the prepared catalysts. The specific surface area of 1V6W/Ti is 50.1 m^2/g and that of 1V6WTi/rGO is 74.2 m^2/g, confirming that the rGO support increases the specific surface area of the catalyst by ~50%. The average pore size of 1V6W/Ti is 22.3 nm and that of 1V6WTi/rGO is 16.3 nm, which is a decrease of ~10%. These results demonstrate that the rGO supported catalysts are composed of smaller particles with higher density, because of an enormous specific surface area of rGO (Table S1). Generally, catalytic activity is closely related to the specific surface area of a catalyst upon which the chemical reaction can take place. Thus, the rGO-supported VWTi catalyst represents a breakthrough in the development of efficient NOx-removal catalysts with lower V_2O_5 and WO_3 content because the rGO provides superior active-component dispersity, uniform particle-size distribution, and high specific surface area.

3. NOx Removal Efficiency Measurement

Fig. 4 shows the NOx-removal efficiencies of the prepared catalysts using NH_3 as a reducing agent at 250 °C≤T_{OP}≤500 °C. The curves reveal that the highest NOx-removal efficiency occurs at T_{OP}=450 °C, and the efficiency is 78% for 1V6W/Ti, 89% for 1V6WTi/rGO, 82% for 0.5V6WTi/rGO, 84% for 1V3WTi/rGO, and 77% for 0.5V3WTi/rGO. The NOx-removal efficiency of the 1V6WTi/rGO catalyst is 11% higher than that of the 1V6W/Ti catalyst. In addition, 1V3WTi/rGO shows a higher NOx-removal efficiency than that for 0.5V6WTi/rGO, which confirms that V_2O_5 is the main active catalytic component for NOx reduction and that WO_3 serves as a promoter. Interestingly, the 0.5V3WTi/rGO catalyst, which was prepared with V_2O_5 and WO_3 content half those of the 1V6W catalysts, shows a similar NOx-removal efficiency to that of the 1V6W/Ti catalyst over the entire temperature range.

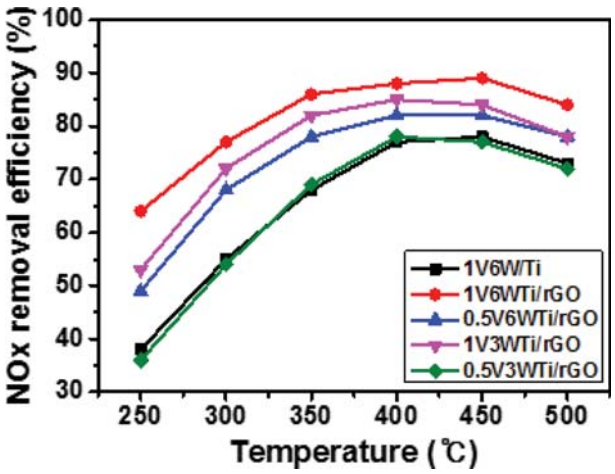

Fig. 4. NOx removal efficiencies of the 1V6W/Ti (black), 1V6WTi/rGO (red), 0.5V6WTi/rGO (blue), 1V3WTi/rGO (magenta), and 0.5V3WTi/rGO (olive) catalysts measured in the temperature range 250-500 °C.

The catalytic reaction with NH_3 over V-based SCR catalysts occurs between the adsorbed NH_3 and gaseous or adsorbed NO, and the main reaction involves the two V species V=O and V-OH at the Brønsted acid sites [32]. Generally, catalytic NOx-removal efficiency can be improved by increasing the content of V and W, which are the active catalytic components for NOx reduction. However, our measurements clearly demonstrate that similar or even higher NOx-removal efficiency can be achieved using an rGO-supported VWTi catalyst with lower V and W content because of its improved particle dispersity, uniform particle-size distribution, and high specific surface area. In addition, SEM and Raman analysis of the catalyst after the NOx-removal measurement were performed to confirm the stability of the VWTi/rGO catalyst at high temperature (Supplementary Material, Fig. S2), and it was demonstrated that no severe changes of VWTi/rGO catalyst were observed after the reaction.

4. Surface Acidity of the Catalysts

To further elucidate the effects of the rGO support, the surface activities of the prepared catalysts were investigated using FT-IR. Fig. 5 shows the FT-IR spectra for the prepared catalysts, and magnifications of the spectra from the ranges 1,700-1,500 cm^{-1} (①) and 1,100-900 cm^{-1} (②). A weak peak at 1,633 cm^{-1} is presented by the 1V6W/Ti catalyst, which is in the range of Brønsted acid sites, and the peak around 1,630-1,640 cm^{-1} is attributed to the bending vibrations of O-H bonds from water molecules adsorbed on the catalyst surface [33]. For the VWTi/rGO catalysts, the 1,633 cm^{-1} peak slightly overlaps with a broad peak at 1,571 cm^{-1}, which is also observed in the spectra of rGO. The peak at 1,571 cm^{-1} is assigned to C=C skeletal vibrations, and the broad peak from 1,250 to 1,100 cm^{-1} is assigned to C-OH stretching vibrations [34]. These peaks are not in the range of Brønsted acid sites and do not correspond to the presence of V. The peak observed near 970 cm^{-1} is charac-

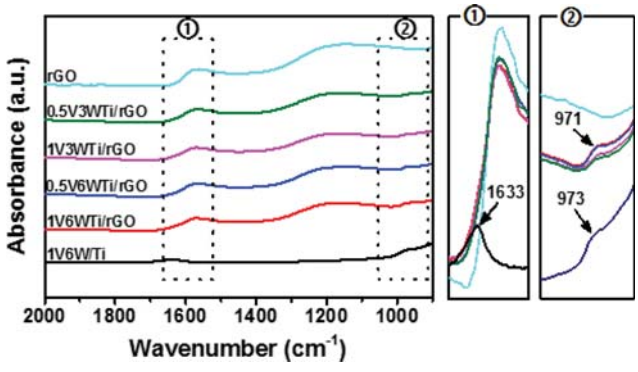

Fig. 5. FT-IR spectra for the 1V6W/Ti (black), 1V6WTi/rGO (red), 0.5V6WTi/rGO (blue), 1V3WTi/rGO (magenta), and 0.5V3WTi/rGO (olive) catalysts and rGO (cyan), and magnifications of the spectra from the ranges 1,700-1,500 cm^{-1} (①) and 1,100-900 cm^{-1} (②).

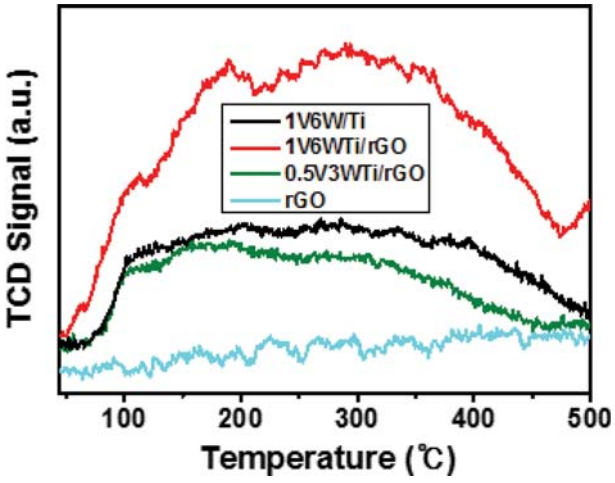

Fig. 6. NH_3-TPD profiles of the prepared 1V6W/Ti (black), 1V6WTi/rGO (red), 0.5V3WTi/rGO (olive) catalysts and rGO (cyan) measured in the temperature range of 50-500 °C.

teristic of V-O bond vibrations [35]. The FT-IR measurements show that the catalysts both with and without the rGO support have similar peak positions related to catalytic activity for NOx conversion, and that rGO is not involved in the catalytic reaction.

Fig. 6 shows the NH_3-TPD profiles of the prepared catalysts measured in the temperature range 50-500 °C. Before the TPD measurements, the temperature of the reactor was increased to 200 °C for 1 h to remove the impurities and moisture present in the samples. NH_3 gas was introduced and adsorbed on the acid sites of the catalysts until saturation. Then, the gas was heated to 800 °C and desorption was detected using a thermal conductivity detector located at the outlet of the reactor. Since the activity of reactions between NH_3 and SCR catalysts is highly related to the density of the active sites on the surface, the adsorption and activation of NH_3 on a catalyst surface is important for obtaining higher catalytic activity [36]. Topsøe et al. proposed that catalytic activity is related to the NH_3 adsorbed on the acid sites associated with V^{5+}-OH and V^{5+}=O [37]. When NH_3 is activated, gas-phase NO reacts with the activated NH_3 to form an intermediate state which decomposes NO into N_2 and H_2O, and the regeneration of active sites is induced by oxygen gas. The TPD measurements indicated physisorbed, weak and strong chemisorption of NH_3. The Brønsted acid sites are produced on the vanadium surface by hydration of V-O-M species. The peak over 300 °C is the desorption of NH_3 at the Brønsted acid site (V-OH) because the desorption of NH_3 on the Brønsted acid site (V-OH) is stronger than that of Lewis acid site [38]. In general, the Brønsted acid site increases with the increase of vanadium content [39], and it was also confirmed that the acid site decreased with the decrease of the vanadium content (0.5%). In addition, the NH_3-TPD data show that desorption of NH_3 from the 1V6WTi/rGO catalyst is superior to that from the 1V6W/Ti catalyst, even though they have the same amount of catalytic components, which agrees with the NOx removal efficiency measurements (Fig. 4). Jo et al. reported that the catalysts with low dispersity have difficulty to obtain high NOx removal efficiency because of the decreased contact between NOx and the catalyst components [40], and the low dispersion of tungsten oxide leads to the reduced the Brønsted acid site of catalyst surface [31]. Thus, the density of acid sites is increased by the presence of the rGO support because of the improved specific surface area and dispersity of the catalytic components.

CONCLUSION

V_2O_5-WO_3-TiO_2/rGO catalysts were successfully prepared by adopting rGO as a catalyst support. The rGO support provides functional sites for the nucleation of nanoparticles, leading to the formation of high-specific-surface-area VWTi catalysts with well-dispersed nanoparticles with a uniform size distribution. The prepared catalysts exhibit similar or even higher NOx-removal efficiency at lower V_2O_5 and WO_3 content, and their catalytic activity was further elucidated with FT-IR and NH_3-TPD measurements. The results reported here may provide useful design considerations for further work on the SCR and other classes of catalytic reaction systems.

ACKNOWLEDGEMENT

We acknowledge financial support from the Ministry of Trade, Industry and Energy of Knowledge Economy (MOTIE) under grant numbers 10052455 and 20152510101820.

SUPPORTING INFORMATION

Additional information as noted in the text. This information is available via the Internet at http://www.springer.com/chemistry/journal/11814.

REFERENCES

1. S. Andreoli, F. A. Deorsola, C. Galletti and R. Pirone, *Chem. Eng. J.*, **278**, 174 (2015).
2. J. Hwang, H. J. Ha, J. Ryu, J. J. Choi, C. W. Ahn, J. W Kim, B. D. Hahn, W. H. Yoon, H. Lee and J. H. Choi, *Catal. Commun.*, **94**, 1 (2017).
3. J. Ko, D. Jin, W. Jang, C. L. Myung, S. Kwon and S. Park, *Appl. Energy*, **187**, 652 (2016).
4. C. Qi, W. Bao, L. Wang, H. Li and W. Wu, *Catalysts*, **7**, 110 (2017).
5. J. P. Chen and R. T. Yang, *Appl. Catal., A*, **80**, 135 (1992).
6. X. Xiao, S. Xiong, B. Li, Y. Geng and S. Yang, *Catal. Lett.*, **146**, 2242 (2016).
7. J.-H. Choi, S.-K. Kim and Y.-C. Bak, *Korean J. Chem. Eng.*, **18**, 719 (2001).
8. R. Q. Long and R. T. Yang, *J. Catal.*, **186**, 254 (1991).
9. B. Li, C. Wu, Y. Li and J. Zhang, *Environ. Sci. Technol.*, **45**, 7394 (2011).
10. X. Wu, Z. Si, G. Li, D. Weng and Z. Ma, *J. Rare Earths.*, **29**, 64 (2011).
11. H. Kamata, S. Ueno, T. Naito and A. Yukimura, *Ind. Eng. Chem. Res.*, **47**, 8136 (2008).
12. G. Madia, M. Elsener, M. Koebel, F. Raimondi and A. Wokaun, *Appl. Catal., A*, **39**, 181 (2002).
13. S. Djerad, L. Tifouti, M. Crocoll and W. Weisweiler, *J. Mol. Catal.*

A: Chem., **208**, 257 (2004).
14. L. Alemany, L. Lietti, N. Rerlazzo, P. Forzatti, G. Busca, E. Giamello and F. Bregani, *J. Catal.*, **155**, 117 (1995).
15. V. A. Ehrlich, A. K. Nersesyan, C. Hoelzl, F. Ferk, J. Bichler, E. Valic, A. Schaffer, R. Schulte-Hermann, M. Fenech, K.-H. Wagner and K. Siegfried, *Environ. Health Perspect.*, **116**, 1689 (2008).
16. H. Turkez, E. Sonmez, O. Turkez, Y. I. Mokhtar, A. Di Stefano and G. Turgut, *Braz. Arch. Biol. Technol.*, **57**, 532 (2014).
17. M. Cao, X. X. Wang, W. Q. Cao and J. Yuna, *J. Mater. Chem. C*, **3**, 6589 (2015).
18. Y. Zhu, S. Murali, W. Cai, X. Li, J. Suk, J. R. Potts and R. S. Ruoff, *Adv. Mater.*, **22**, 3906 (2010).
19. W. Su, X. Lu, S. Jia, J. Wang, H. Ma and Y. Xing, *Catal. Lett.*, **145**, 1446 (2015).
20. K. K. Lee, S. Deng, H. M. Fan, S. Mhaisalkar, H. R. Tan, E. S. Tok, K. P. Loh, W. S. Chin and C. H. Sow, *Nanoscale*, **4**, 2958 (2012).
21. P. Wang, Y. Zhai, D. Wang and S. Dong, *Nanoscale*, **3**, 1640 (2010).
22. S. Mao, S. Cui, G. Lu, K. Yu, Z. Wen and J. Chen, *J. Mater. Chem.*, **22**, 11009 (2012).
23. M. A-Romero, R. Camposeco, S. Castillo, J. Marin, V. R-Gonzalez, Luz A. G-Serrano and I. M-CenTeno, *Fuel*, **198**, 123 (2017).
24. V.-K. Nguyen, J.-H. Park, C.-H. Shin, *Korean J. Chem. Eng.*, **31**, 582 (2014).
25. D. W. Kwon, K. B. Nam and S. C. Hong, *Appl. Catal., A*, **497**, 160 (2015).
26. VGB Technical Association of Large Power Plant Operators, Guideline for the testing of deNOx catalysts, VGB PowerTech, Essen (1998).
27. X. Lu, C. Song, C.-C. Chang, Y. Teng, Z. Tong and X. Tang, *Ind. Eng. Chem. Res.*, **53**, 11601 (2014).
28. S. Shen, X. Wang, T. Chen, Z. Feng and C. Li, *J. Phys. Chem. C*, **118**, 12661 (2014).
29. B. Shen, T. Liu, N. Zhao, X. Yang and L. Deng, *J. Environ. Sci.*, **22**, 1447 (2010).
30. H. K. Matralis, Ch. Papadopoulou, Ch. Kordulis, A. Elguezabal and V. Corberan, *Appl. Catal., A*, **126**, 365 (1995).
31. C. Wang, S. Yang, H. Chang, Y. Peng and J. Li, *Chem. Eng. J.*, **225**, 520 (2013).
32. I. Nova and E. Tronconi, Urea-SCR Technology for deNOx After Treatment of Diesel Exhausts, Springer, New York (2014).
33. P. Kongsong, L. Sikong, S. Niyomwas and V. Rachpech, *Sci. World J.*, **2014**, 869706 (2014).
34. H. Zheng, C. Y. Neo, X. Mei, J. Qiu and J. Ouyang, *J. Mater. Chem.*, **22**, 14465 (2012).
35. I. Mjejri, N. Etteyeb and F. Sediri, *Mater. Res. Bull.*, **48**, 3335 (2013).
36. S. Wang, T. Guo, W. Pan, M. Li, P. Sun, S. Liu, S. Liu, X. Sun and J. Liu, *Phys. Chem. Chem. Phys.*, **19**, 5333 (2017).
37. N.-Y. Topsøe, J. A. Dumesic and H. Topsøe, *J. Catal.*, **151**, 241 (1995).
38. X. Du, X. Gao, K. Qiu, Z. Luo and K. Cen, *J. Phys. Chem. C*, **119**, 1905 (2015).
39. C.-H. Lin and H. Bai, *Appl. Catal., B*, **42**, 279 (2003).
40. S.-H. Jo, B. Shin, M.-C. Shin, C. J. Van Tyne and H. Lee, *Catal. Commun.*, **57**, 134 (2014).

Supporting Information

Reduced graphene oxide supported V_2O_5-WO_3-TiO_2 catalysts for selective catalytic reduction of NOx

Minwoo Lee[*,], Bora Ye[*], Bora Jeong[*], Hye-yeon Chun[*], Duck Hyun Lee[*], Sam-sik Park[***], Heesoo Lee[**], and Hong-Dae Kim[*,†]**

*Green Materials & Processes Group, Ulsan Regional Division, Korea Institute of Industrial Technology, Ulsan 44413, Korea
**Department of Materials Science and Engineering, Pusan National University, Busan 46142, Korea
***R&D Center, NANO. Co., Ltd., Sangju 37257, Korea
(*Received 12 March 2018 • accepted 24 June 2018*)

Fig. S1 showing SEM and TEM image and Raman spectrum of the rGO surface, also the specific surface area of rGO was analyzed by BET in the Table S1. Furthermore, the phase of the vanadium and tungsten is oxidized into V_2O_5, WO_3 of the prepared catalysts confirmed by XRF in the Table S2.

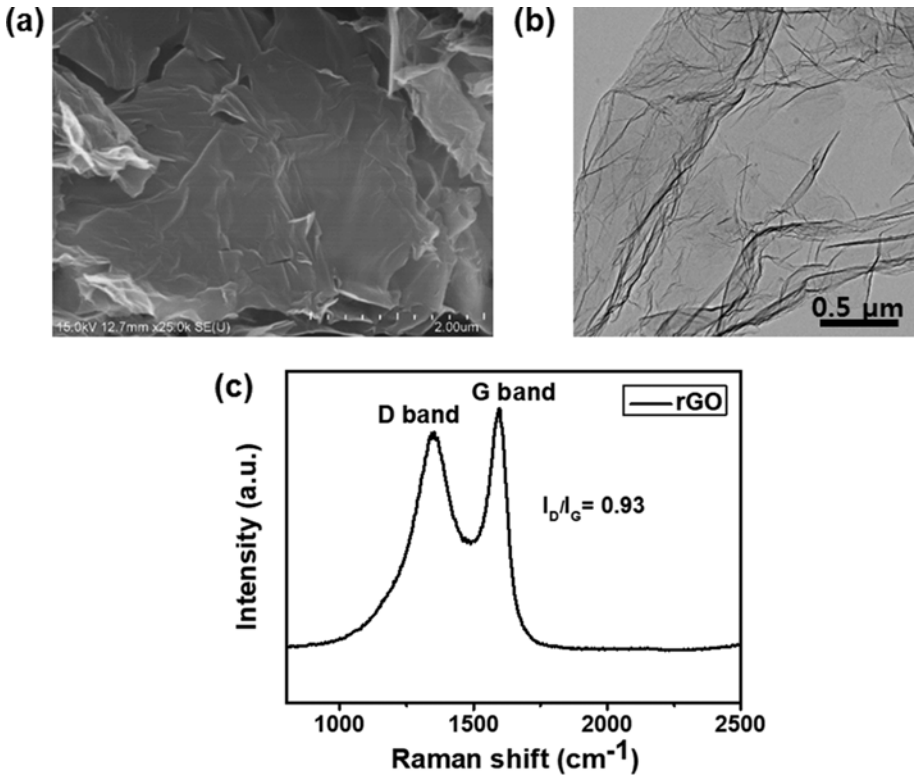

Fig. S1. (a) SEM and (b) TEM images of a reduced graphene oxide (rGO) surface. (c) Raman spectrum of rGO. The D band centered at 1,345 cm^{-1} represents surface defects and disorder, and the G band at 1,594 cm^{-1} is characteristic of sp^2 carbon. The intensity ratio of the two peaks (i.e., ID/IG) is used to estimate the degree of order or disorder in graphitic materials.

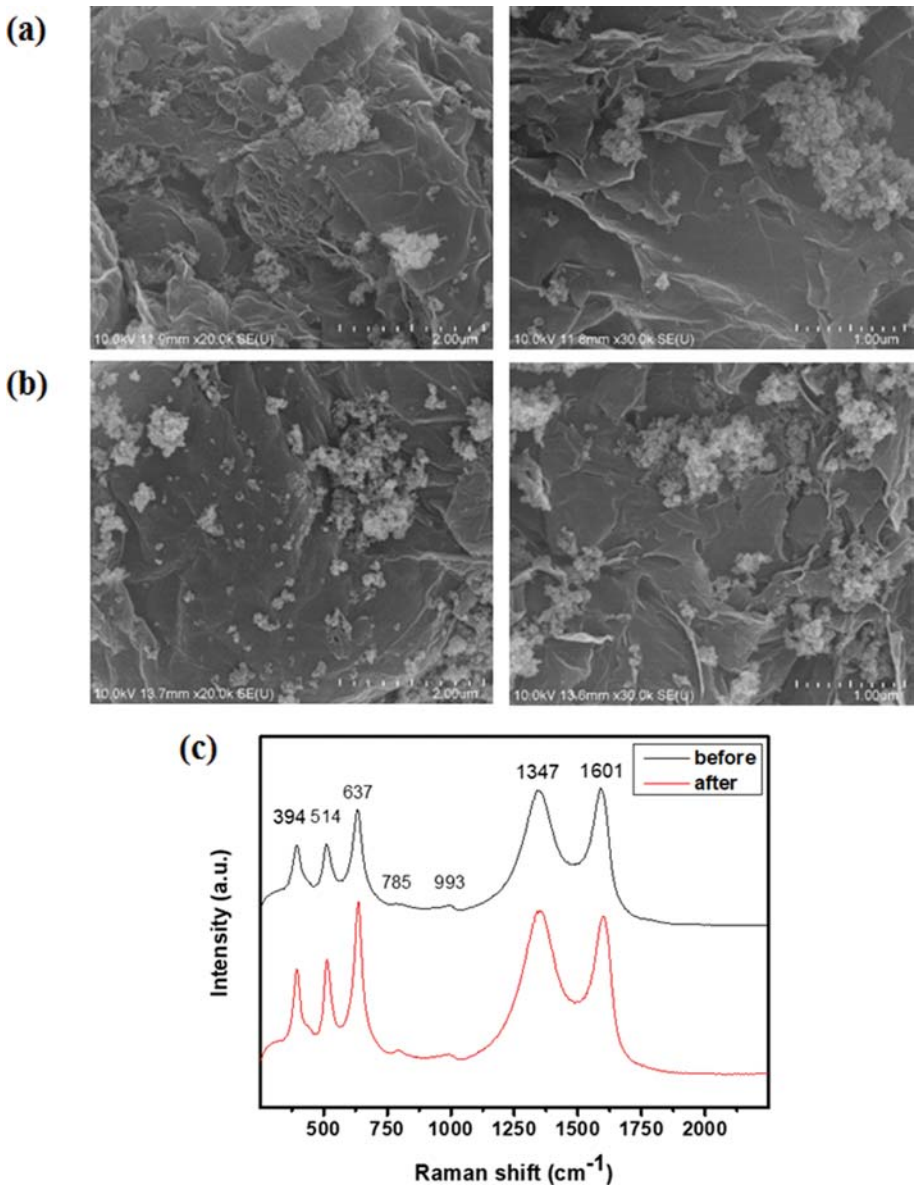

Fig. S2. The surface of the used 1V6WTi/rGO catalyst (a) before reaction (before) and (b) after reaction at 450 °C for 10 h (after), (c) the Raman spectrum of the 1V6WTi/rGO catalyst before and after reaction at the operating temperature 250<T_{OP}<500 °C.

Table S1. Physicochemical properties of rGO analyzed by BET

Samples	S_{BET} [m^2g^{-1}]	Pore volume [cm^3g^{-1}]	Average pore size [nm]
rGO	233.29	0.56	9.82

Table S2. Compositions (in wt%) of the prepared catalysts as revealed by X-ray fluorescence spectroscopy (XRF)

Samples	Al_2O_3	SiO_2	SO_3	TiO_2	WO_3	V_2O_5
1V6W/Ti	0.012	0.019	0.009	93.697	5.228	1.019
1V6WTi/rGO	0.013	0.039	0.041	93.741	5.092	1.018
0.5V6WTi/rGO	0.010	0.040	0.034	94.518	4.922	0.499
1V3WTi/rGO	0.013	0.037	0.060	96.221	2.608	0.983
0.5V3WTi/rGO	0.008	0.040	0.047	96.657	2.665	0.491